11-2008

Comparison of Measured and Modeled Temporal Coherence of Sound Near 75 Hz and 3683 km in the Pacific Ocean

John L. Spiesberger
University of Pennsylvania, johnsr@sas.upenn.edu

Suggested Citation:
Spiesberger, J.L. (2008). "Comparison of measured and modeled temporal coherence of sound near 75 Hz and 3683 km in the Pacific Ocean." *Journal of the Acoustical Society of America.* **124** (5). pp. 2805 - 2811.

Comparison of Measured and Modeled Temporal Coherence of Sound Near 75 Hz and 3683 km in the Pacific Ocean

Abstract
The hypothesis to test is internal gravity waves following a Garrett–Munk spectrum are sufficient to explain temporal coherence of sound at 3683 km in the Pacific Ocean for a signal at 75 Hz and a pulse resolution of 0.03 s. Signals from a 20 min transmission are collected on a towed array. After correcting the data for what likely appears to be acceleration of the receiver, the probability distribution for multipath coherence time is very similar to that obtained from Monte Carlo simulations of the impulse response. The most likely coherence time is 20 min, the longest that can be measured with a 20 min transmission. Predictions of multipath temporal coherence and amplitude fluctuations appear accurate enough to make useful predictions of channel capacity.

Disciplines
Physical Sciences and Mathematics

Comments
Suggested Citation:
Spiesberger, J.L. (2008). "Comparison of measured and modeled temporal coherence of sound near 75 Hz and 3683 km in the Pacific Ocean." *Journal of the Acoustical Society of America.* **124** (5). pp. 2805 - 2811.

Comparison of measured and modeled temporal coherence of sound near 75 Hz and 3683 km in the Pacific Ocean

John L. Spiesberger
Department of Earth and Environmental Science, 240 S. 33rd Street, University of Pennsylvania, Philadelphia, Pennsylvania 19104-6316

(Received 10 August 2007; revised 24 July 2008; accepted 28 July 2008)

The hypothesis to test is internal gravity waves following a Garrett–Munk spectrum are sufficient to explain temporal coherence of sound at 3683 km in the Pacific Ocean for a signal at 75 Hz and a pulse resolution of 0.03 s. Signals from a 20 min transmission are collected on a towed array. After correcting the data for what likely appears to be acceleration of the receiver, the probability distribution for multipath coherence time is very similar to that obtained from Monte Carlo simulations of the impulse response. The most likely coherence time is 20 min, the longest that can be measured with a 20 min transmission. Predictions of multipath temporal coherence and amplitude fluctuations appear accurate enough to make useful predictions of channel capacity.
 [DOI: 10.1121/1.2977676]

PACS number(s): 43.30.Re [WC] Pages: 2805–2811

I. INTRODUCTION

Temporal coherence of low-frequency sound is important for detection, location, acoustic communication, acoustical oceanography, and theoretical studies. We estimate coherence with a passive towed research array. Signals originate from an acoustic source (75 Hz and 0.03 s resolution) at Kauai[1] at 3682.5 km distance (Fig. 1). We test the hypothesis that coherence can be predicted from fluctuations of internal gravity waves obeying the Garrett–Munk spectrum.[2,3] Standard methods in acoustics and oceanography are used with no effort to fit models to data. A Monte Carlo technique yields time-varying impulse responses at the receiver by evolving the internal wave field with a linear dispersion relation. We adopt a minimalist approach toward the understanding causes of coherence. Unless a strong inconsistency is found between the model and data, there is not a strong reason to include additional phenomenon or modify model parameters. In this and previous works,[4,5] parameters are taken from original literature without modification. If temporal scales from this experiment agree with the model, it would be the model's third success[4,5] out of four attempts. The fourth attempt was inconclusive because the experimental analysis by others appears to be not quite complete.[6] Using different models in another experiment, comparison of temporal coherence of acoustical mode one was confounded by difficulty in removing motion of instruments.[7] However, when instruments do not move, or when their role can be well enough understood, Monte Carlo methods appear to yield accurate estimates of coherence. Particularly important may be applications in communication, where adaptive methods are commonly used to suppress effects from instrumental motion.

II. EXPERIMENT AND DATA PROCESSING

Data come from an acoustic source at Kauai[1] and a towed array in the Gulf of Alaska (Fig. 1). The source is placed at the bottom at 816 m depth at 22.349 °N, 200.43033 °E. The power, timing, and transmission characteristics are controlled by connecting the source by cable to a computer on land. Its time base is linked to an atomic standard. A broadband signal is transmitted at a center frequency of 75 Hz. Carrier phase is modulated every two cycles using a linear maximal shift register sequence having 1023 digits. First zeros in the emitted spectrum are at $75/2=37.5$ Hz on either side of 75 Hz. The pulse resolution is $1/37 \sim 0.027$ s.

The signal periodicity and level are $(1023)2/75 = 27.280$ s and 195 dB *re* 1 μPa at 1 m, respectively. At 04:00 Greenwich Mean Time on 6 September 2002, the source transmitted 44 consecutive periods lasting 20 min. See Ref. 1 for details on the transmitted code.

The receiver is a horizontal array towed at 131 m depth at 53.5219302 °N, 215.319727 °E. Location is written with greater precision than its accuracy of a few kilometers. This precision is given so others can model this section with identical coordinates. It is not possible to compare with models absolute time of signal propagation between the source and the receiver with O(1) km error.

The geodesic length is 3682.6 km from source to receiver (Fig. 1). During signal arrival, the array speed is 0.2 m/s with heading at 286 °T. Since the bearing angle of the geodesic at the receiver is 25.9 °T, the incoming signal makes an angle of 80.1° with respect to ship heading. During 20 min of data reception, the ship travels 0.24 km and is 0.041 km closer to the source at the end of 20 min.

III. MODELS

A. Environment

The section of sound speed is computed using Del Grosso's algorithm[8] and Levitus' climatological averages[9] of temperature and salinity for summer. The depth of minimum speed varies from 800 m at the source to 90 m at the receiver. Since the acoustic models use Cartesian coordinates, the sound speed profiles are translated to Cartesian coordinates using the Earth-flattening transformation.[10]

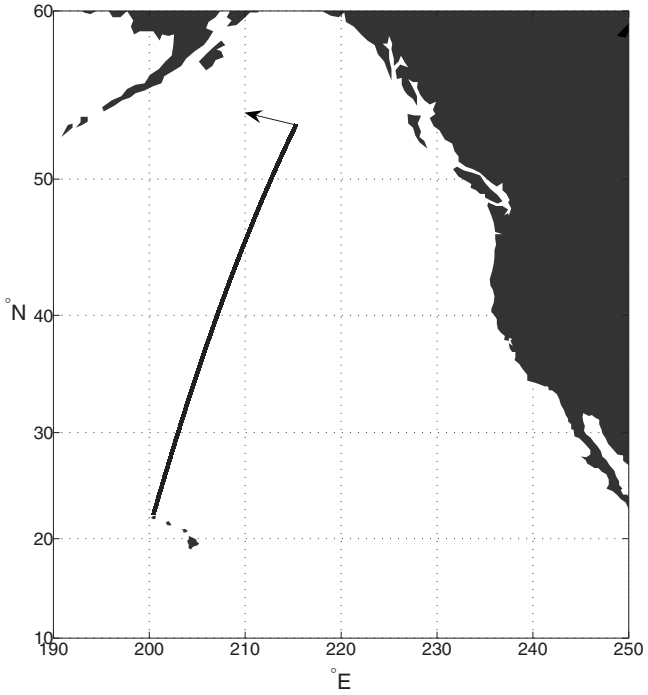

FIG. 1. Geodesic between Kauai source and towed receiver with heading shown.

Internal waves are modeled with the complete Garrett–Munk[2,3] spectrum. It differs slightly from the method by Colosi and Brown[11] who used WKB scaling to obtain internal wave modes in the vertical coordinate. We solve the equation without WKB scaling. Reference 12 completely describes the model used here.

Currents are ignored, being two orders of magnitude less than sound speed perturbations arising from adiabatic vertical displacements of water in the upper ocean. Perturbations are added to climatology of sound speed described above. The internal wave modes are precomputed and retrieved as needed at range intervals of 80 km to account for changes in water depth, buoyancy frequency, and sound speed. The vertical displacements of modes are set to zero at surface and bottom. For each 80 km interval, a three-dimensional field of internal waves is computed in a box of 80×80 km^2 by D m, where D is the average depth of ocean in that interval. A vertical slice through the box gives vertical displacements along the geodesic for any desired section. Temporal evolution of the field is governed using the linear dispersion relation. Energy of the internal wave field is taken to be that specified by Garrett and Munk.[2,3]

Bathymetry along the section consists of a steeply sloping region on the slope of Kauai, followed by an abyssal region with seamounts (Fig. 2). Within 100 km of the source, bathymetry is measured with a Seabeam survey[13] (B. Howe, personal communication). A bathymetric database is used elsewhere.[14]

The parabolic approximation of the acoustic wave equation requires parameters to define acoustic propagation in the seabottom. Those chosen (not shown) may or may not be close to those at the site. Other values would very likely not significantly change coherence times of modeled multipath. They would likely change their amplitudes, but this does not seem to be important for comparing the measured and modeled probability distributions of coherence time.

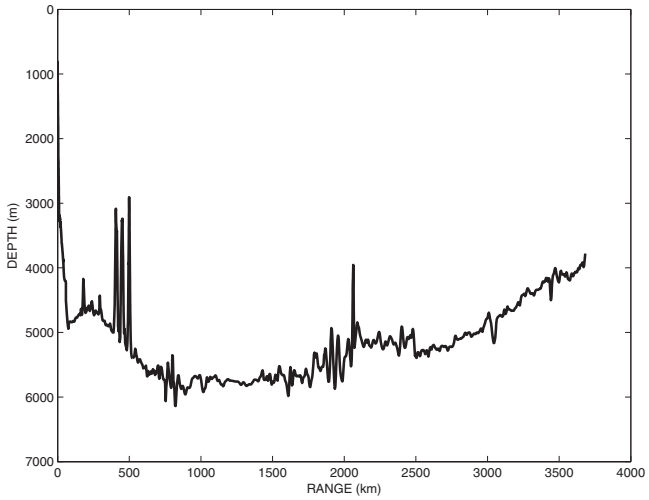

FIG. 2. Bathymetry between acoustic source at 0 km and receiver.

B. Acoustic models

Fans of rays are traced using a program, ZRAY, that is a modification of ray.[15] Eigenrays are found using another program. These programs have been used to identify acoustic paths before.[16] Rays reflect specularly from the bottom. Both geometric and nongeometric arrivals are found. Geometric types are those that pass through the source and receiver. Nongeometric types are those that provide energy at the receiver on the shadow sides of caustics. For lack of a more reliable value, rays that reflect from the bottom suffer an attenuation of 3 dB/bounce. The sound speed field used for tracing rays is identical to that used for the sound speed insensitive parabolic model[17] at its computational grid (below).

This parabolic approximation[17] computes a two-dimensional field of sound along the geodesic from 0 to 8000 m depth. Tests suggest that travel times of pulses are computed with an accuracy of a few milliseconds.[17] The impulse response is computed by applying an inverse Fourier transform to many single-frequency computations. Vertical slices of sound speed are obtained from a three-dimensional field of internal waves (Sec. III A). Numerical convergence is obtained by halving grid sizes until the answers do not change significantly. Parameters chosen lead to convergence of a normalized cross-correlation coefficient of 0.99 or greater. We use a vertical grid spacing of 1.95 m. The horizontal grid spacing varies between 33 and 150 m. A separation of 33 m is used when bathymetry is steep near source and seamounts.

IV. IMPULSE RESPONSE

Using standard techniques, a nonadaptive time-domain beamformer is used to steer a beam toward the source. The beam is much wider than any variation in signal direction. Next, each separate 27.280 s M-sequence period is adjusted for various Doppler corrections and correlated with a replica of the transmitted sequence.[18] Replica correlation with a linear maximal shift register sequence compresses 27.280 s of

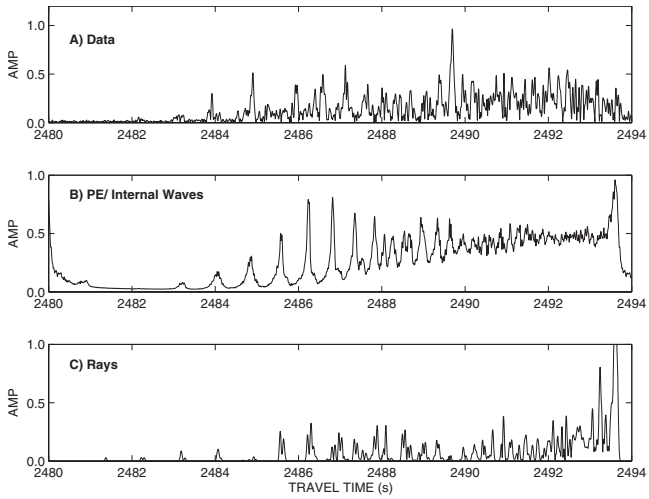

FIG. 3. Comparison between measured (a) and modeled impulse responses [(b) and (c)], each on its own arbitrary amplitude scale. Travel times of data are shifted to approximately correspond with models. The parabolic approximation model (b) is the result of incoherently averaging 150 impulse responses through an evolving field of internal waves. The ray model (c) does not incorporate fluctuations from internal waves.

energy from each acoustic path into a pulse of duration $2/75=0.02667$ s with a theoretical gain of $10\log_{10}(1023)=30$ dB.

Search in Doppler space is done to maximize the average signal-to-noise ratio of multipath due to an equivalent relative speed between the source and the receiver. Search increment is fine enough that one discerns changes of an average multipath signal-to-noise ratio of 0.1 dB or less near optimum correction. Individual fading of any single acoustic path is not caused by this procedure We obtain sufficient signal-to-noise ratio to examine the impulse response. To avoid end effects, 42 of 44 transmitted periods are processed, with the first and last unused.

Peak signal-to-noise ratio varies within the 42 periods between 20 and 25 dB (not shown). After applying an optimum Doppler correction for each period, the peak signal-to-noise ratio is 33 dB in the coherent average of these 42 periods [Fig. 3(a)]. A standard weighted average,

$$\bar{x}=\frac{\Sigma_{i=1}^{42}x_i/\sigma_i^2}{\Sigma_{i=1}^{42}1/\sigma_i^2},$$

is used to emphasize periods with higher signal-to-noise ratios, where σ_i^2 is the noise variance of the ith M-sequence period. If all 42 periods had the same signal-to-noise ratio, a $10\log_{10}42=16$ dB gain would be obtained over any individual period when the noise was uncorrelated and the signal was perfectly correlated. The gain to 33 dB in the weighted coherent average, from 20 to 25 dB/period, is a bit less than ideal. Earliest paths arrive near 2483 s and end just before 2494 s [Fig. 3(a)].

The parabolic approximation[17] is used to compute 150 realizations of impulse response at 4 min intervals through a time-evolving field of internal waves. White Gaussian noise is added to each impulse response having about the same peak signal-to-noise ratio as data. When the record-averaged peak signal-to-noise ratio is 20 dB, the incoherent average of the model has about the same time extent as measured (Fig. 3(b)]. Modeled energy between 2480 and 2482 s comes from periodicity of the impulse response obtained by Fourier transforming a finite number of frequencies.

If we had measurements of the impulse response over a day or longer, previous research indicates that likely good correspondence would be found between incoherently modeled and measured impulse responses.[16,19] However, a single measurement is not enough to show up all paths, many of which intermittently fade due to fluctuations in the sea.

The impulse response from ray theory also has about the same time extent as observed [Fig. 3(c)]. Rays are traced through climatological variations without internal waves. Amplitude of the final set of rays is truncated from 1.9 to unity near 2494 s so amplitudes of weaker arrivals can be seen more easily. Earliest arriving rays have upper turning depths varying from about 240 m near the source to 10–50 m near the receiver. Rays arriving last have upper turning depths varying from about 750 m near the source to 60–70 m near the receiver. These ray depths gradually rise as sound travels into colder waters where depth of minimum sound speed shoals. Most clumps of arriving energy are composed of temporally unresolved rays.

We did not trace rays through an internal wave field to avoid effects of ray chaos. Effects of internal waves on sound are better portrayed with the parabolic approximation[17] [Fig. 3(b)].

V. TEMPORAL CORRELATION

A. Doppler corrections

In Sec. IV, we found that all 42 impulse responses could be coherently averaged to increase signal-to-noise ratio over that for any individual impulse response after separately correcting each for Doppler. The fact that a Doppler shift is needed begs the question as to the roles of receiver motion and ocean in setting coherence time. We do not have accurate enough estimates of receiver speed to separately remove its effects. In a previous experiment with stationary source and towed array, we found coherence time to be insensitive to Doppler speed correction used during reception of various M-sequences.[5] For example, one could use the best Doppler speed correction for the first M-sequence period to correct the remaining periods. This result yielded coherence times that looked like those obtained by separately correcting each M-sequence period. This likely happened because tow speeds were quite steady. We are not so lucky in this experiment. Velocity of the receiver appears to change enough so that we cannot use a Doppler correction from the first period to correct the remaining periods without seriously affecting the estimates for coherence time (not shown). Consequently, there is less information concerning the ocean's role in limiting coherence time.

The array is towed at 0.2 m/s nearly perpendicular to direction to the source. Doppler corrections are small, starting at 0.0886 m/s for the first M-sequence period and ending at -0.0125 m/s for the last. The decrease is not monotonic but shows a definite and gradual trend toward lower speeds during 20 min of reception (not shown). The source lies on

the ocean bottom, so the first thing to check is whether these Doppler corrections are primarily due to acceleration of the receiver or fluctuations in the sea.

Change in sonic travel time due only to acceleration a of a receiver in geophysical time interval $\delta\tau$ is

$$\delta t_a = a\delta\tau^2/(2c), \tag{1}$$

where c is the signal speed, $a=\delta v/\delta\tau$, and change in Doppler speed is δv. For oceanographic causes, consider a barotropic current over distance R of form $u=u_0 \cos \omega\tau$, where u_0 is the magnitude and ω is the radian frequency. The effect of this current on travel time is $\delta t_u=-uR/c^2$ to first order. Change in travel time in interval $\delta\tau$ due to the temporal change of the current is

$$\Delta\delta t_u = u\omega R\delta\tau \sin(\omega\tau)/c^2, \tag{2}$$

with the maximum value found for $\sin \omega\tau=1$. Equating maximum value of Eq. (2) with δt_a, we find

$$\frac{u_0 R}{T} = c\delta v/4\pi, \tag{3}$$

where $T=2\pi/\omega$. For the observed Doppler changes of $\delta v=0.1$ m/s and $c\sim1479$ m/s, the right side of Eq. (3) is 11.8 m^2/s^2. As for the left side, typical values of barotropic currents in open ocean are 0.01 m/s over scales of the basin, so take $R=3600$ km, and consider a semidiurnal period of 12 h. Then the left side is $0.01\times3.6\times10^6/(12\times3600)=0.8$ m^2/s^2. This is an order of magnitude smaller than the 11.8 m^2/s^2 needed to account for a 0.1 m/s change in Doppler.

At ocean-basin scales, nonstationary oscillations in the north Pacific lead to changes in travel time between a few and tens of milliseconds at periods between 2 and 20 h.[20] These measurements appear to be the only other oceanographic candidate that might explain change in Doppler. The origin of the oscillations is unknown, but u_0R/T can be estimated since we know T and $u_0R=-c^2\delta t$. For $T=2$ h and $\delta t=0.002$ s, $u_0R/T\sim0.6$ m^2/s^2. For longer periods, $T=20$ h and $\delta t=0.01$ s, so $u_0R/T\sim0.3$ m^2/s^2. Both are an order of magnitude too small to account for 11.8 m^2/s^2 needed to account for observed changes in Doppler. Section V C below will explain why the GM spectrum[2] itself does not account for observed corrections in Doppler. We conclude that observed 0.1 m/s change in Doppler is probably due to acceleration of the receiver.

B. Data

With one 20 min transmission, there are many fewer degrees of freedom to estimate coherence time than a different experiment where transmissions were continuous for five days.[4] The previous experiment computed a standard normalized correlation coefficient of coherence time of the entire impulse response lasting 4 s. In this paper, degrees of freedom are increased by considering coherence of many small windows of arrival time from each of 42 impulse responses. We also use a different definition of coherence time. We might have used a traditional definition of coherence time based on a lag yielding a normalized correlation coefficient of e^{-1}. However, we see below that many paths are coherent even at the longest explorable lag of 20 min.

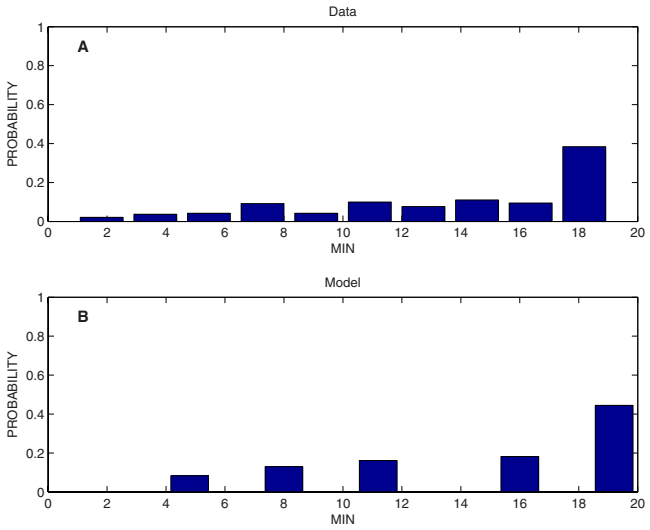

FIG. 4. (Color online) (a) Probability of temporal coherence within 380 analysis windows of 0.03 s each covering 11.4 s duration of the entire measured impulse response. Probability that any analysis window has the given coherence time is shown up to 19.06 min (42 M-sequence periods). Each M-sequence period is separately pre-processed for the best Doppler correction yielding highest average signal-to-noise ratio in the impulse response. (b) Same as (a) except computed from modeled impulse responses without any Doppler correction. Average peak signal-to-noise ratio in the model is set to 20 dB, about the same as measured.

As explained before, the data are Doppler corrected to suppress acceleration of the receiver. The resulting impulse response for each of 42 periods is subdivided into 380 windows of travel time of duration 0.03 s each, which is about the temporal resolution of the transmitted signal. Windows are chosen to cover energetic arrivals lasting 10 s. For each window, we compute the peak signal-to-noise ratio from each coherent average,

$$a(t,m) = \frac{1}{m}\sum_{i=1}^{m} r_i(t), \quad m = 1,2,3,\ldots,42, \tag{4}$$

where $r_i(t)$ is the real-valued time series at the receiver within one window, and t is the arrival time. Letting $\hat{m}$ denote the value of m yielding the maximum signal-to-noise ratio, coherence time is defined as $T=\hat{m}27.628/60$ min. For example, if the coherent average of the first eight M-sequence periods has largest signal-to-noise ratio, the coherence time is $8\times27.628/60$ min ($m=8$). An empirical probability distribution is plotted for these 380 windows [Fig. 4(a)]. The most likely coherence time is 19 min. It occurs with a probability of 0.4. Lesser coherence times are distributed between 2 and 16 min. Coherence time of the signal may be longer than 19 min, but we cannot explore this possibility with 42 transmissions of this M-sequence.

It is sometimes thought that signal-to-noise ratio of a coherent integration increases monotonically to some peak then decreases. However, rise to maximum need not occur monotonically.[6] In this experiment, signal-to-noise ratio often does *not* increase monotonically. For example, signal-to-noise ratio decreases for the largest peak in the impulse response at about 1 min and again at 6 min of integration time

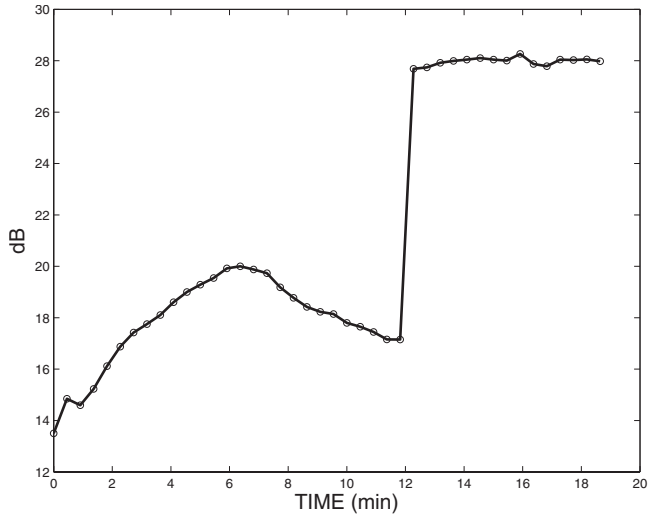

FIG. 5. Signal-to-noise ratio vs time of coherent integration. The window corresponds to the largest peak in the impulse response of the data [Fig. 3(a)]. The circles occur at intervals equal to the M-sequence period (27.280 s).

before rising to 28 dB near 12 min (Fig. 5). Considering 380 windows of arrival time, many coherence times decline before eventually rising (not shown). The model exhibits similar behavior (not shown). Temporary decreases in signal-to-noise ratio are not due to sudden increase in noise. Instead, noise varies little during any of the 42 M-sequences (Fig. 6). Neither model nor data show signal-to-noise ratio increasing monotonically with number of periods m as $10\log(m)$ dB. Our definition of coherence time does not depend on whether signal-to-noise ratio increases monotonically.

We found no significant difference in coherence time between the early and late energies. Both have coherence times with probability distributions similar to that in Fig. 4(a) (not shown). Window width is increased from 0.03 to 0.09 s to investigate if coherence time changes. Coherence time could decrease with a number of independent multipath in the window. However, there is no significant difference from that in Fig. 4(a) with a 0.09 s window (not shown). Evidently, there are not significantly more independent oscillations in a 0.09 s than 0.03 s window.

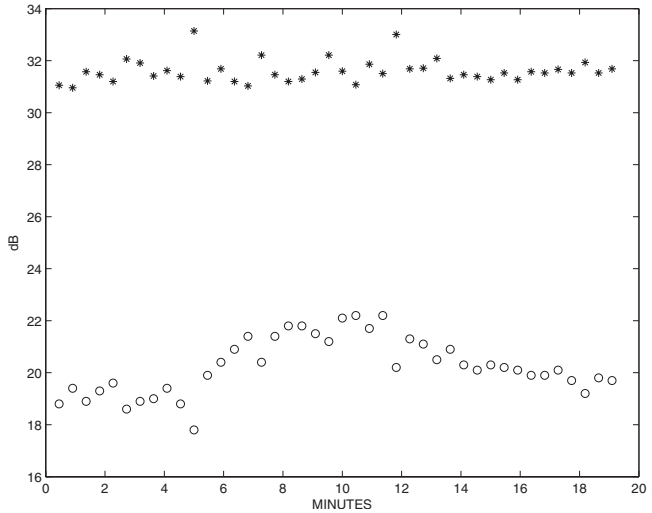

FIG. 6. Standard deviation of noise (*) and average signal-to-noise ratio of biggest 80 peaks (o) for each of 42 M-sequence periods for optimum Doppler correction. Both quantities are in dB.

C. Model

The parabolic approximation[17] yields an impulse response for 150 records at 4 min intervals. (Internal waves evolve by 4 min between computations.) Each impulse response is subdivided into $W \equiv 365$ adjacent windows of width 0.03 s. This covers the modeled impulse response lasting 10 s (Fig. 3(b)). White Gaussian noise with mean zero and variance σ^2 is added to each record. Signal-to-noise ratio of each realization is the same as the data in the following sense. Let peak amplitude of record j be $\hat{a}_j$, $j = 1, 2, 3, \ldots, 150$. The record-averaged peak amplitude is $\bar{a} = 150^{-1}\Sigma_{j=1}^{150}\hat{a}_j$. Variance is determined by solving for σ^2 in $20 = 10\log_{10}(\bar{a}^2/\sigma^2)$(dB). This ensures that record-average peak signal-to-noise ratio is the same as measured.

A bootstrap scheme is used to estimate the coherence time for each of 365 windows. First, we select at random $B = 3000$ different starting records among 150 possibilities. Direction of the coherent average is selected at random to go forward or backward in geophysical time with respect to starting record. A total of five records are added together in the randomly chosen direction. End point problems are handled by choosing a direction that would not extend below 1 or above 150. With five records, we explore coherence times up to 5 records $\times$ (4 min/record) = 20 min. For each starting record, coherence time is computed by selecting the number of records n, yielding largest signal-to-noise ratio where n can go from 1 to 5. Coherence time is $4n$ min. Letting coherence time for bootstrap b of travel time window k be T_{bk}, there are $BW = 3000 \times 150 = 450\,000$ estimates of T_{bk}. An empirical probability distribution is computed from these [Fig. 4(b)]. It resembles that from data. The most likely coherence time is 19 min, occurring with a probability of 0.4. Histogram bars have slightly different centers for model and data because model and data are available at 240 and 27.28 s intervals, respectively. The results are almost the same if the record-average signal-to-noise ratio is 25 instead of 20 dB (not shown).

The GM spectrum does not account for Doppler corrections of 0.1 m/s. To see why, we estimate the average change in acoustic travel time between each of 150 impulse responses using the phase and amplitude of each model output. The technique is described elsewhere.[20] Travel times change by less than 0.001 s between the 1st and 150th records, which is a tenth of a cycle at 75 Hz. This is too small to cause observed Doppler corrections.

Of 365 modeled windows, many have coherence times of at least 2 h (not shown). Figure 4 is limited to 20 min because that is the limit imposed by experiment. It is important to analyze model and data the same way.

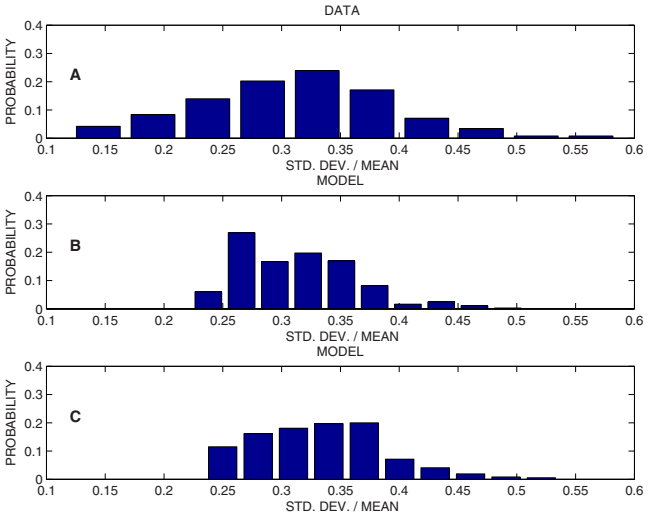

FIG. 7. (Color online) Same as Fig. 4 except for amplitude fluctuations. Within each window, mean and standard deviation of amplitude are computed. Their ratio yields f in Eq. (5), which gives values for the horizontal axis. Data are in A. Models for 20 and 25 dB signal-to-noise ratio are in panels B and C, respectively.

VI. AMPLITUDE FLUCTUATIONS

A. Data

Analysis of amplitude fluctuations is made in each of 380 windows discussed in Sec. V B. For each window, there are 42 realizations of peak amplitude, a_k, $k=1,2,3,\ldots,42$. We compute

$$f \equiv \mathrm{Std}[a_k]/\mathrm{Mean}[a_k], \tag{5}$$

where Std and Mean denote the standard deviation and the mean, respectively. This statistic is useful for computing channel capacity for some types of wireless acoustic modems in the sea.[5] We have 380 values of f, one for each window. An empirical probability distribution shows a peak near 0.35 with minimum and maximum values of 0.15 and 0.55 [Fig. 7(a)]. For informational purposes, we state that Eq. (5) is different than a scintillation index.

B. Model

Analysis of amplitude fluctuations is made in each of 365 windows discussed in Sec. V C. Noise is added to each of 150 records as before. For each window, we compute f from Eq. (5) except k goes to 150 model records. Empirical probability distribution of f differs somewhat from that derived from measurements [Fig. 7(b)]. Resemblance is better if we set record averaged peak signal-to-noise ratio to 25 dB [Fig. 7(c)]. Perhaps 25 dB better mimics average signal-to-noise ratio.

VII. DISCUSSION

Despite the fact that we have only one 20 min signal to work with, a means is found to increase reliability of statistical estimates by subdividing arriving energy into small windows with a duration of 0.03 s. Coherence times from individual windows are most likely near 20 min regardless of whether early or late energy is considered, or whether the window duration is 0.03 or 0.09 s. The model has many more degrees of freedom than the data. The model has snapshots of impulse response for 10 h at 4 min intervals.

Two issues seem to pertain to acoustic communication systems. First, they are often implemented by using differential Doppler to correct signals from different paths. In this experiment, it appears unnecessary to differentially correct paths for Doppler. A single Doppler correction at 27.28 s intervals is sufficient to yield coherence times between 2 and 19 min (Fig. 3). Second, the predicted values of probability distributions of coherence time and fractional amplitude are needed to predict channel capacity for some types of underwater modems.[5] Our predictions appear to be realistic enough to be useful for predicting channel capacity. Predicting the channel capacity is beyond the scope of this paper.

We do not know how to be sure what limits coherence time for signals lasting tens of minutes when receiver motion compels us to remove Doppler effects for each separate period of an M-sequence. In a separate experiment with the same source signal and different towed array in the same region, the observed and predicted coherence times agreed by correcting instrument motion for a single Doppler speed.[5] That array was towed at steadier speed. We will never know, but it does seem plausible that variable speed corrections used here do not affect the estimates of coherence time limited by the ocean. Effects of tides, other oscillations of the Pacific at shorter periods, and internal gravity waves are a factor of 10 too small to cause observed Doppler shifts (Secs. V A and V C). Receiver acceleration is the only phenomenon that could plausibly cause observed variation of Doppler. Whatever the cause, the corrected time series has a probability distribution of coherence time that looks very similar to that obtained from a standard model based on internal gravity waves alone.

It is reassuring to have a systematic method that yields coherence times similar to observed, at least here and in two other experiments checked so far.[4,5] Theories to date do not appear to be able to accurately predict coherence times.[4] If it turns out that Monte Carlo simulations of coherence time based on a standard spectrum of internal waves yield reliable coherence times in many experiments, a foundation will exist for further developing theory.

It seems possible that probability distribution for coherence time could extend past 20 min. We have not addressed whether coherence time exceeds 20 min since the hypothesis is untestable with a 20 min signal. What seems to be important is that modeled probability distribution for coherence time looks like that derived from data.

Finally, the Monte Carlo impulse responses are run on a supercomputer. Others are working on faster methods for implementing Monte Carlo approaches.[21]

ACKNOWLEDGMENTS

This research was supported by the Office of Naval Research Contract No. N00014-06-C-0031 and by a grant of computer time from the DOD High Performance Computing Modernization Program at the Naval Oceanographic Office. The ZRAY raytrace program was modified from the program

written by James Bowlin. I thank reviewers for their suggestions.

[1]B. M. Howe, S. G. Anderson, A. B. Baggeroer, J. A. Colosi, K. R. Hardy, D. Horwitt, F. W. Karig, S. Leach, J. A. Mercer, K. Metzger, L. O. Olson, D. A. Peckham, D. A. Reddaway, R. R. Ryan, R. P. Stein, K. von der Heydt, J. D. Watson, S. L. Weslander, and P. Worcester, "Instrumentation for the acoustic thermometry of ocean climate (ATOC) prototype Pacific Ocean network," Proceedings of the OCEANS 95 Conference Proceedings, San Diego, CA, 9–12 October 1995, pp. 1483–1500.

[2]C. Garrett and W. Munk, "Space-time scales of internal waves," Geophys. Fluid Dyn. **3**, 225–264 (1972).

[3]C. Garrett and W. Munk, "Space-time scales of internal waves: A progress report," J. Geophys. Res. **80**, 291–297 (1975).

[4]J. L. Spiesberger, F. Tappert, and A. R. Jacobson, "Blind prediction of broadband coherence time at basin-scales," J. Acoust. Soc. Am. **114**, 3147–3154 (2003).

[5]J. L. Spiesberger and D. Green, "Statistical characterization of very low frequency communication channels at ocean basin-scales," Proceedings of the MTS-IEEE Oceans '06 Conference, Boston, 2006, Paper No. 060322-06, pp. 1–6.

[6]J. L. Spiesberger, "Numerical prediction of coherent integration time at 75 Hz, 0.03 temporal resolution at 3250 km," Proceedings of the MTS-IEEE Oceans '06 Conference, Boston, 2006, Paper No. 060323-02, pp. 1–4.

[7]K. Wage, M. Dzieciuch, P. Worcester, B. Howe, and J. Mercer, "Mode coherence at megameter ranges in the North Pacific Ocean," J. Acoust. Soc. Am. **117**, 1565–1581 (2005).

[8]V. A. Del Grosso, "New equation for the speed of sound in natural waters with comparisons to other equations," J. Acoust. Soc. Am. **56**, 1084–1091 (1974).

[9]S. Levitus, "Climatological atlas of the world ocean," NOAA Professional Paper No. 13, U. S. Government Printing Office, Washington, DC, 1982.

[10]A. Ben-Menahem and S. J. Singh, *Seismic Waves and Sources* (Springer-Verlag, New York, 1981), p. 1108.

[11]J. A. Colosi and M. G. Brown, "Efficient numerical simulation of stochastic internal-wave-induced sound-speed perturbation fields," J. Acoust. Soc. Am. **103**, 2232–2235 (1998).

[12]M. A. Wolfson and J. L. Spiesberger, "Full wave simulation of the forward scattering of sound in a structured ocean: A comparison with observations," J. Acoust. Soc. Am. **106**, 1293–1306 (1999).

[13]V. Renard and J. P. Allenon, "Sea Beam, multi-beam echo-sounding in "Jean Charcot:" Description, evaluation and first results," Int. Hydrogr. Rev **56**, 35–67 (1979).

[14]Naval Oceanographic Office Data Model, Oceanographic and Atmospheric Master Library (OAML), Digital bathymetric database variable resolution (DBDB-V), Version 5.1, April, 2006.

[15]J. B. Bowlin, J. L. Spiesberger, and L. F. Freitag, "Ocean acoustical ray-tracing software RAY," Woods Hole Oceanographic Technical Report No. WHOI-93-10, 1992.

[16]J. L. Spiesberger, "An updated perspective on basin-scale tomography," J. Acoust. Soc. Am. **109**, 1740–1742 (2001).

[17]F. Tappert, J. L. Spiesberger, and L. Boden, "New full-wave approximation for ocean acoustic travel time predictions," J. Acoust. Soc. Am. **97**, 2771–2782 (1995).

[18]S. W. Golomb, *Shift Register Sequences* (Holden-Day, San Francisco, CA, 1967).

[19]J. L. Spiesberger, R. C. Spindel, and K. Metzger, "Stability and identification of ocean acoustic multipaths," J. Acoust. Soc. Am. **67**, 2011–2017 (1980).

[20]J. L. Spiesberger, P. J. Bushong, K. Metzger, and T. G. Birdsall, "Ocean acoustic tomography: Estimating the acoustic travel time with phase," IEEE J. Ocean. Eng. **14**, 108–119 (1989).

[21]A. K. Morozov and J. A. Colosi, "Stochastic differential equation analysis for ocean acoustic energy scattering by internal waves," J. Acoust. Soc. Am. **119**, 3344(2006).